http://wrap.warwick.ac.uk

1   G. Boscato, C. Casalegno, S. Russo and J. T. MOTTRAM, 'Buckling of built-up columns of

2   pultruded FRP C-sections,' *Journal of Composites for Construction*,

3   http://ascelibrary.org/doi/abs/10.1061/%28ASCE%29CC.1943-5614.0000453

4

5   **Buckling of Built-up Columns of Pultruded FRP C-sections**

6   Giosuè Boscato[1], Carlo Casalegno[2], Salvatore Russo[3], and J. Toby Mottram[4]

7

8   **ABSTRACT**

9   This paper presents the test results of an experimental investigation to evaluate the buckling

10 behaviour of built-up columns of pultruded profiles, subjected to axial compression.

11 Specimens are assembled using four (off-the-shelf) channel shaped profiles of E-glass Fibre

12 Reinforced Polymer (FRP), having the similar detailing as strut members in a large FRP

13 structure that was executed in 2009 to start the restoration of the Santa Maria Paganica

14 church in L'Aquila, Italy. This church had partially collapsed walls and no roof after the 2009

15 April 6th earthquake of 6.3 magnitude. A total of six columns have been characterised with

16 two different configurations for the bolted connections joining together the channel sections

17 into a built-up strut. Test results are discussed and a comparison is made with closed form

18 equation predictions for flexural buckling resistance, and with buckling resistances

19 established from both Eigenvalue and geometric non-linear finite element analyses. Results

20 reported and discussed show that there is a significant role played by the end loading

21 condition, the composite action and imperfections. Simple closed form equations are found to

22 overestimate the flexural buckling strength, whilst the resistance by the non-linear analysis is

[1]Ph.D., Department of Construction, IUAV University of Venice, Dorsoduro 2206, 30123 Venice, Italy. E-mail:
gboscato@iuav.it
[2]Ph.D., Department of Construction, IUAV University of Venice, Dorsoduro 2206, 30123 Venice, Italy
(corresponding author). E-mail: carlo.casalegno@polito.it
[3]Associate Professor of Structural Civil Engineering, Department of Construction, IUAV University of Venice,
Dorsoduro 2206, 30123 Venice, Italy. E-mail: russo@iuav.it
[4]Professor, School of Engineering, University of Warwick, Coventry CV4 7AL, UK. E-mail:
J.T.Mottram@warwick.ac.uk

23   seen to give a reasonably reliable numerical approach to establishing the actual buckling

24   behaviour.

25   **SUBJECT HEADINGS**: Buckling, pultruded built-up columns, laboratory tests, finite

26   element analysis

27   **INTRODUCTION**

28   The use of Fibre Reinforced Polymer (FRP) shapes and systems in construction has

29   significantly increased in recent years. The increased interest lies in the advantages over

30   traditional construction materials, such as high strength-to-weight ratio, corrosion resistance

31   and the ease of transportation and erection (Mottram 2011).

32   Pultrusion is a composite manufacturing process for the continuous production of FRP thin-

33   walled shapes. One category of Pultruded (PFRP) profiles possess the same cross-sectional

34   shapes (I, H, Leg-angle, channel, box, etc.) as found in structural steelwork, but these

35   standard profiles are not as large, and have very different mechanical and structural properties

36   (Bank 2006). They consist of E-glass fibre reinforcement having layers of unidirectional

37   rovings and continuous mats in a thermoset resin based matrix, usually of a polyester or

38   vinylester polymer resin. Having a weight of only 25% of steel these profiles offer

39   lightweight structural solutions. Like steel, the tensile strength in the longitudinal direction is

40   more than 200 MPa. The longitudinal modulus of elasticity lies in the range 20-30 GPa,

41   which is 10-6 times lower than steel. The elastic modulus in the transverse direction is 0.3 of

42   the longitudinal value. The expected range for the in-plane shear modulus of elasticity of

43   PFRP material is 3 to 5 GPa.

44   The mechanical performance of individual PFRP structural profiles for frame members has

45   received attention by researchers (Bank 2006; Russo 2007; Boscato & Russo 2009; Boscato

46   *et al*. 2011). This is not the situation for built-up (column) members subjected to concentric

47   loading, and this form of member is the subject of a fact finding study reported in this paper.

48   The predominantly linear elastic mechanical properties of PFRP material (Bank 2006) leads

49   to different column response because there is neither material yielding nor gross plasticity

50   deformation. For the same cross-section dimensions the thin-walled PFRP column (of 'I' or

51   'H' shape) has the potential to fail first with a local instability buckling mode (Mottram

52   2004). Moreover, the buckling response is more related to the actual geometry of the cross-

53   section than to the member's slenderness (however this non-dimensional column length is

54   established). In general, PFRP columns of open-sectioned shape ('H' or 'I') will be subjected

55   to failure by global (flexural) buckling of the member or by local (plate) buckling of the

56   flange outstands (Barbero, Dede and Jones, 2000: Lane and Mottram 2002; Mottram, Brown

57   and Anderson 2003).

58   The local instability mode causes outstands to rotate about their intersection junction with the

59   web; this is particularly true for the wide flange (or 'H') profiles with height and breadth of

60   same dimensions. It has been shown via experimental investigations that axially compressed

61   H- and I-shapes can give one of two distinct types of failure, with local buckling occurring in

62   'shorter' columns that do not crush first, and flexural buckling prevailing when the member's

63   effective length classify the column as 'slender'. For intermediate slendernesses the two

64   instabilities may coexist and there might be imperfection sensitive modal coupling interaction

65   that leads to a tertiary buckling mode. Lane and Mottram (2002) have shown from axial

66   column tests with H-shapes that modal coupling lowers the buckling resistance by a few

67   percent in the transition range for column lengths between the two distinct modes of elastic

68   buckling.

69   Several research groups have contributed towards the development of knowledge to

70   understand the elastic buckling response of PFRP columns of standard shapes. From the

71   plethora   of   sources   (refer   to   literature   database   at:

72   www2.warwick.ac.uk/fac/sci/eng/staff/jtm/pfrp_latest.pdf) a number of investigations of note

73 are by Barbero *et al.* (2000), Pecce and Cosenza (2000), Hashem and Yuan (2001), Lane and

74 Mottram (2002), Di Tommaso and Russo (2003), Mottram (2004) and Turvey and Zhang

75 (2006). None of the previous studies involved a built-up column member and so the study

76 reported in this paper is novel and will add to what we know and understand. Because of

77 practical limitations in processing capabilities the maximum size for an 'off-the–shelve'

78 PFRP has a cross-section area of about 13000 mm^2 (for a I-profile of 610 x 178 x 12.7 mm).

79 The advantage of the built-up fabrication option is that it would allow bigger cross-sectional

80 sized members to be used in structural/civil engineering projects.

81 The structural response might be even more complex for a built-up column that is fabricated

82 from joining together (individual) standard PFRP profiles by a method of mechanical

83 fastening. Complexity could increase because of the possible interaction of buckling modes

84 within the individual shapes and the influence of composite action between them. Moreover,

85 the presence of material, geometrical and 'loading' imperfections is likely to have a influence

86 on how the built-up member responds and fails, when subjected to concentric compression

87 loading.

88 Presented in this paper are the test results from an experimental investigation to address and

89 evaluate the buckling characteristics of a PFRP built-up column. The column's detailing is

90 similar to strut members in the 1050 m^2 by 30 m high FRP structure located inside the church

91 of Santa Maria Paganica in L'Aquila (Russo, Boscato and Mottram 2012; Russo 2012). This

92 church lost its roof and parts of the masonry walls in the 6th April 2009 earthquake and, until

93 government funds are available for the restoration work, its fragile interior requires protection

94 from the weather. The engineered solution formulate in 120 days (Russo *at al*. 2012) was to

95 execute a temporary structure of FRP material (and at 8 kg per m^2 it is a light weight

96 solution). To understand the measured responses the column failure results are compared

97   with resistances from closed form equations for flexural buckling and numerical results from

98   Eigenvalue (bifurcation buckling) and geometrical non-linear finite element analyses.

99

100   **DESCRIPTION OF BUILT-UP STRUT**

101   The goal of this study is to investigate the structural performance of a built-up member,

102   subjected to uniform compression, similar to those adopted in the construction of the

103   L'Aquila FRP structure shown in Figures 1(a) and 1(b). Shown in Figure 1(b) is the structural

104   system chosen to address the important design issues of second-order effects in ULS design

105   and to provide a suitable configuration for the (M14 steel) bolted gusset plate joints. Frame

106   jointing is characterized by using FRP components manufactured by two different composite

107   processing methods. The gusset plating (for in-plane isotropic properties) seen in Figure 1(b)

108   was manufactured using the bag molding process. The strut members are assembled from

109   four off-the-shelf pultruded channel-shaped sections having same cross-section dimensions

110   (152 x 43 mm) and wall thickness of 9.5 mm.

111   Figure 2(a) shows the tested built-up member's cross-section (envelop is 152 x 171 mm)

112   comprising four channel (C) profiles, with two (back-to-back) for the web and two for the

113   flanges. Connections between the channels were made using M10 (stainless) steel bolting in 1

114   mm clearance holes. Bolts were tightened to a torque of 45 Nm. The two Cs for the web of

115   6.5 mm thickness were connected using two bolts and packing plates at spacings of $1/3^{rd}$ (911

116   mm) and $2/3^{rd}$ (1822 mm) along the column's length (*L* is 2734 mm). As seen in Figure 2(a)

117   there is a bolted connection between a flange in the web and the web of a channel for the

118   member's flange. In column testing the compressive force is ('uniformly') applied directly

119   into the web's two C-profiles with an area of 3000 mm^2. The two Cs forming the flanges are

120   present to increase the built-up column's lateral flexural stiffness.

121 Geometrical and physical properties for the strut member are reported in Table 1. Column (1)

122 defines the property and Column (2) gives its notation. Listed in Column (3) are the cross-

123 section's properties (to three significant figures) for a constant ('Nominal') wall thickness of

124 9.5 mm in the four channels. This is the cross-section size for struts, see Figure 1, in the

125 L'Aquila temporary structure (Russo *at al*. 2012). The equivalent properties in Column (4)

126 are for the cross-section used in the experimental ('Exp') investigation, as it comprised three

127 Cs of 6.5 mm thickness (two web and one flange) and one flange C with thicker walls at 9.5

128 mm thickness. The justification for the asymmetric cross-section about the major-axis of

129 bending was to trigger second-order effects from onset of the compression loading.

130

131 **EXPERIMENTAL INVESTIGATION**

132 The static test configuration for the experimental investigation is illustrated in Figure 2.

133 Figure 2(a) shows the overall column specimen, which can be with or without the third-

134 length (at $L/3$ and $2L/3$) bolting (see Figure 2(d)) between the web and the flange Cs. It also

135 shows that at the mid-height section there are eight axial strain gauges (SG1 to SG8) and two

136 displacement transducers numbered [18] and [19]. Images in Figures 2(b) and 2(c) show that

137 the hinge-hinge end condition is realized by using a steel sphere placed between 'rigid' steel

138 plates in contact with the PFRP specimen and testing machine. A specimen is placed in the

139 testing machine so that the centre of the cross-sections area is closely aligned with the

140 compression load path. The end fixture allows for unrestrained global flexural or flexural-

141 torsional instability deformation to occur.

142 This fact finding test series involved the two column configurations with labels CFG1 and

143 CFG2, having three specimens per batch. CFG1 is for the built-up member with full bolting

144 at four cross-section levels and CFG2 is for without bolting at the two $1/3^{rd}$ height locations.

145 Removal of the bolting was to facilitate the release of the composite action between the web

146   and flange Cs, and can be expected to expose the effectiveness of using spaced bolt rows in

147   built-up members. Note that the equivalent bolting located close to the two free ends cannot

148   be removed. One objective of the study was to establish the level of composite action from

149   having made the design decision to have bolting at the $1/3^{rd}$ length spacing.

150   Compression force was applied using a computer controlled universal testing machine of 600

151   tonne (6000 kN) capacity. To measure the (longitudinal) response the specimen, at $L/2$ (1367

152   mm), has the eight strain gauges (SG1 to SG8) shown in Figure 2(a). SG1, SG2 and SG6 are

153   on the flange C-section of 9.5 mm thickness, whilst SG3 to SG5 are on the other flange C-

154   section of 6.5 mm thickness. Gauges SG7 and SG8 are positioned at the centre of the two

155   back-to-back Cs forming the the web. Measurement of lateral displacement along the Minor-

156   axis and Major-axis planes was made using displacement transducers. Transducers [18] and

157   [19] are located at mid-height. For the flexural deformation about the Minor-axis there is

158   third transducer, labeled [20], that is located at $L/4$ (684 mm) (see Fig. 2(a)). Because the

159   half-wave length(s) for potential local instabilities was unknown no transducers were

160   involved with the requirement to pick-up deformation signaling local buckling failure. The

161   origin for the length of the column specimen is at the base of the specimen.

162

163   **Test Results**

164   Results for the two column configurations of CFG1 and CFG2 are plotted in Figures 3 to 8.

165   Figures 3 to 5 are for the three CFG1 specimens, whilst Figures 6 to 8 are for the three CFG2

166   columns. In each of the figures, part (a) reports, at $L/2$, the axial strains from SG1 to SG 8,

167   and part (b) gives the lateral displacements at $L/4$ from [20] and at $L/2$ from [18] and [19] for

168   the Major axis and Minor axis components. The plot axes are the same in part (a) for the

169   compressive strain and average compressive stress (with σ positive), calculated using the

170   (mid-height) cross-section area A from Column (4) in Table 1. The compressive stress given

171   in the figures is for the axial compression load alone. It does not therefore represent the

172   highest fiber compression stress due to the combination of axial and flexural deformations.

173   Because the flexural deformation can occur in two directions about the principal axes the

174   abscissa axis in part (b) of Figures 3 to 8 is specific to the test. To highlight the load carrying

175   capacity of the columns the ordinate axis in part (b) is for the applied compression force.

176   The eight strain gauge readings in Part (a) of Figures 3 to 5 show that the CFG1 cross-section

177   in tests 1 to 3 is initially compressed with a fairly uniform compressive stress. Significant

178   divergence between the eight stress-strain curves is recorded when the load exceeds 55 kN

179   (or 8.3 MPa) in test 1 (Figure 3), 117 kN (or 17.8 MPa) in test 2 (Figures 4) and 78 kN (or

180   11.8 MPa) in test 3 (Figure 5). Below this transition state the difference between the

181   minimum and maximum strains is 52%, 47% and 36% respectively. Afterwards the presence

182   of deformations associated with individual-section flexural buckling and/or built-up member

183   flexural buckling radically alters a column's response. This behavior causes a sudden

184   increase in the difference between the minimum and maximum strains to 86%, 80% and 83%.

185   The main difference in response is observed by a relatively higher increase in the SG7 and

186   SG8 strains for the two web Cs. One reason to explain this observation is that the

187   compression loading is only applied over the web area. The flanges are free from the

188   externally applied load and are only influenced by the composite action (force transfer) at the

189   rows of bolting. Another reason is found from analyzing the results of the Eigenvalue

190   buckling analysis as it shows SG7 and SG8 are positioned in a region with relative lower

191   flexure strains.

192   The specific lateral deformation curves plotted in Figure 5(b) for CFG1 test 3 shows that the

193   (negative) displacement measured by transducer [20] at $L/4$, *c.f.* with [19], was actually

194   picking-up a deflection from the pronounced development of a C-section flexural buckling

195   failure. In CFG1 test 1 (Figure 3(b)) and CFG1 test 2 (Figure 4(b)) the equivalent

196   displacements recorded by [19] at *L/2* and at *L/4* by [20] were registering a deformation for a

197   failure by overall global (flexural) buckling. It is noted that flexural buckling of individual

198   flange Cs is also being identified by the displacement measurements from transducer [18] at

199   *L*/2.

200   It was found that the CFG1 columns in tests 1 and 2 ultimately failed by local crushing at one

201   end. Photographs for this failure mechanism from tests 1 and 2 are given in Figures 9(a) and

202   9(b), respectively. It is noted that based on the ratio of cross-sectional areas the average stress

203   over the web area (of 3000 mm^2) at rupture is 1.8 times the average stress given in Figure

204   3(a) and 4(a). Crushing was not the expected mode of ultimate failure and its existence in

205   more than one specimen shows that load transfer into the ends of web was not uniform during

206   testing. Such non-uniformity in the stress field from the presence of geometric imperfections

207   (here from specimen and mounting fixtures on test machine) can be expected on site. It is

208   important to recognize that design for member resistance based on assuming uniform stress

209   could lead to a unsafe member that might fail with a mode not designed against.

210   From the strain gauges data reported in Figure 3(a) it is observed that the increased

211   transversal stiffness in CFG1 test 1, guaranteed by having the 1/3rd height bolting, has

212   prevented an asymmetric distribution of the direct strain profiles in the two flanges of 9.5 and

213   6 mm thickness. It is found that there is strong evidence for a nearly uniform response in the

214   full built-up section. A different strain distribution in the two flange thicknesses is observed

215   in Figures 4(a) and 5(a) for tests 2 and 3. For these CFG1 columns there is a strain divergence

216   within a group of three gauges of 60% in test 2 and 50% in test 3. This change in response is

217   showing the presence, only in the thinner flange section, of second-order deformations.

218   Taking the three strain readings from the thicker flange gauges it is seen that the difference is

219   less, at 50% in test 2 and 25% in test 3.

220   The measured responses of the three CFG2 columns are presented in Figures 6 to 8. As seen

221   from the curves plotted in Figures 6(a) and 7(a) there is a linearly increasing (uniform) stress

222   at mid-height up to 40 kN (or 6 MPa). On further increasing compression the strain curves

223   commence their divergence due to the non-linear response, and when one of the strain gauges

224   recorded a tensile response it was signaling the onset of global (flexural) buckling. From

225   measurements and visual inspection it is observed that, as a consequence of forces being

226   transferred from the web Cs into the flanges through the bolting only at the ends, flexural

227   deformation is induced in the flanges about the member's Major-axis plane and there is

228   torsional deformation too. This form of buckling response was not seen in test 3. This CFG2

229   column was found to fail by local crushing at one end.

230   The reduced transversal stiffness in configuration CFG2, after removal of the bolting,

231   allowed for the generation of flexural buckling and torsional deformations in both flanges.

232   Evidence for this change in response from the CFG1 columns is seen by the higher

233   divergence in the group of strain reading reported in part (a) of Figures 6 and 7.

234   Because there is a very noticeable reduction in column axial stiffness for CFG2 test 1 in

235   Figure 6(b) and test 2 in Figure 7(b) when the load is above 40 kN the response has

236   dramatically changed by the presence of flexural buckling of the individual flange Cs that are

237   no longer connected to the web at the third-lengths.

238

239   **COLUMN ANALYSIS**

240   A preliminary evaluation of the resistances of the two column configurations was made using

241   three different numerical approaches with the PFRP material taken to be linear elastic (Bank

242   2006). In what follows there is a presentation on using the Engesser (1889) closed form

243   equation, and Eigenvalue (for bifurcation buckling) and geometrical non-linear finite element

244   analyses. The latter analysis provided numerical stresses and displacements for a comparison

10

245   with the measured direct stress-lateral displacements via the strains measured by gauges SG1

246   and SG8 and the *y*-displacement from gauge [19].

247   Taking into account the shear deformability of FRP material the closed form equation to

248   predict the critical elastic (flexural) buckling resistance (P_{Esh}) is

249    $$P_{Esh} = \frac{\pi^2 E_z I_x}{\left(k^2 + u\right)\left(kL\right)^2} \quad .$$ (1)

250   In Equation (1), $E_z I_x$ is the flexural rigidity about the Minor-axis of deformation, k is the

251   effective length factor, and u is the shear flexibility parameter, given by $\dfrac{1}{A_{s,x} G_{zx}} \dfrac{\pi^2 E_z I_x}{\left(kL\right)^2}$, with

252    $A_{s,x} G_{zx}$ the member's shear rigidity. The Engesser's equation is a modification to the well-

253   known Euler formula that is for the shear rigid situation (i.e. when u is set to zero).

254   To calculate P_{Esh} the longitudinal modulus of elasticity (E_z) and in-plane shear modulus of

255   elasticity (G_{zx}) of the PFRP are taken from Table 2. These elastic constants are not measured

256   coupon values for the C-section in the testing programme. For this fact finding study the

257   authors decided to perform the analysis using the (lower) Design Manual values (Fiberline

258   2013) because this presented how the strut members were designed in the L'Aquila structure;

259   the only PFRP frame know with built-up members. The required geometric properties of A, I_x

260   and $A_{s,x}$ are those listed in Column (4) in Table 1. The effective length factor k is assumed to

261   be 1.0 to account for hinged ends in the columns having $L = 2734$ mm.

262   Two finite element models, using Ansys® software (Ansys 2011), were developed to simulate

263   the column configurations of CFG1 and CFG2. Salient information towards the finite element

264   (FE) modelling methodology is given next. A goal of the FE work was to obtain reliable

265   numerical results without recourse to needing a mesh possessing an excessive number of

266   degrees of freedom (d.o.f.). The FE mesh specification is shown in Figure 10. The *z*-axis

267   coincides with the member's longitudinal axis and the *x*-y plane is in the plane of the cross-

11

268   section. Flange and web Cs were meshed over their mid-plane surfaces by four-node

269   quadrilateral shell elements. The shell element type was SHELL181, which can model the

270   linear elastic response of orthotropic materials in thin-walled sections. Regions of shell

271   elements to create the model were automatically meshed using the mapped meshing

272   algorithm (Ansys 2011).

273   The bolted connections joining the four C sections were modelled by rigid beam elements of

274   type BEAM188. They were manually assigned when building the mesh specification. At the

275   two $1/3^{rd}$ lengths there were six bolts (see Figure 2(d)), with two in a vertical column to

276   connect the back-to-back Cs forming the web. At the ends of the member there were only the

277   four bolts that are used to join the four web flange outstands to the webs in the two Cs

278   forming the flanges. The location of this bolting in the x-y plane is illustrated in Figure 2(a).

279   At the free ends the web (which extends beyond the free end of the flanges) was connected to

280   a 'rigid' square plate that is perpendicular to the longitudinal axis of the member. To model

281   the full specimen length of 2734 mm a rigid beam element, of length 45 mm is fixed to each

282   plate and aligned with the member's z-axis. The mesh specification had been formulated in

283   such a way to ensure that nodal locations corresponded exactly to bolt hole positions and to

284   where the displacement transducers are located.

285   Nodal d.o.f. at the end of the 'extension' beams were restrained in a way that models the two

286   hinges found in the experimental set-up illustrated in Figure 2. At the extreme ends, where

287   the compressive load was applied, the translational d.o.f.s in the x-direction and y-direction

288   and the rotation degree of freedom around the z-axis were restrained. Applied in the z-

289   direction, for the initial load factor, is a unit (compressive) load of 1 kN. At the other end of

290   the column model the translational degree of freedom in the z-direction was also fully

291   restrained to complete the displacement boundary conditions.

292   The linear elastic FRP is taken to be transversely isotropic (i.e. the behaviour is the same in

293   the *x*- and *y*-directions), with the orthotropic elastic constants listed in Column (3) of Table 2.

294   Notation for the elastic constants in Column (1) is given in Column (2).

295   The Eigenvalue solution was carried out using the block Lanczos algorithm (Ansys 2011).

296   For the two simulations of CFG1 and CFG2 the first buckling mode results were extracted.

297   For column-type CFG1 the predicted critical elastic buckling is 230 kN. The buckled (mode)

298   shape is shown in Figure 11 by way of a contour plot along the length of the column for the

299   nodal displacements in the *y*-direction. The first (Eigenvalue) mode is characterized by

300   Minor-axis global (flexural) buckling of the flanges, accompanied by global flexural buckling

301   of the web C-sections between the bolt rows. Because a bifurcation analysis has been carried

302   out the numerical displacements do not represent the actual test displacements. The contour

303   plots presented in the three figures do allow a qualitative understanding towards the overall

304   buckling response of the built-up member with composite action from bolting at the third

305   lengths.

306   For configuration CFG2 (without bolting at the 1/3rd and 2/3rd lengths) the predicted critical

307   buckling load is much lower at 39 kN. The buckled shape is illustrated in Fig. 12(a) and, as

308   expected, it is dominated by flexural buckling of the thinner (6.5 mm) flange C section. At

309   17% of the CFG1 bifurcation load the significantly lower resistance has to be due to the

310   removal of the very beneficial influence of the composite action from having bolting at the

311   two 1/3rd length levels in CFG1. The CFG2 bolting detailing has therefore been shown to

312   have increased the buckling length of a flange C-section for flexural buckling failure to occur

313   first, and at a compression force that is five times lower than measured in CFG1 test 3 (see

314   Fig. 5).

315   Parts (b) and (c) of Fig. 12 present the Eigenvalue second and third mode shapes for CFG2,

316   with contour plotting for the *x*- and *y*-displacement, respectively. The relevance of presenting

317   the higher mode shapes is that they are used to define the geometric imperfections and an

318   essential contact pairing (restraining C-section separation) in the modelling methodology for

319   the non-linear FE simulations to follow.

320   A geometric non-linear FEA was also conducted in order to better understand the response of

321   the two column configurations over the loading range. The basic FE model was the same

322   described for the Eigenvalue analysis. For the non-linear analysis the compressive load was

323   applied at one end of the model through consecutive steps. The analysis was performed by

324   applying the automatic load stepping option that enables ANSYS® to choose the non-linear

325   solution options, such as: the type of equation solver, the Newton-Raphson solution options,

326   the convergence criteria, the maximum number of iterations. Because the choice of these

327   options influences the speed and numerical precision of the computational solution it was a

328   prudent modeling decision to let the code decide the progression of the non-linear analysis to

329   a buckling mode of failure.

330   In order to execute the non-linear analysis, geometric imperfections were generated

331   consistently with the experimentally observed buckled shapes reproduced in the Eigenvalue

332   analysis. Imperfections are automatically generated by ANSYS® updating the geometry of

333   the FE mesh as a function of a scaling factor related to the mode shapes selected from those

334   computed and illustrated in Figs. 11 and 12. For the generic scaling factor, given notation s,

335   the FE modeling geometry is updated in such a way to have a maximum value of the

336   geometric imperfection equal to s (in the units for the FE mesh), where the position for the

337   maximum amplitude was established from the Eignevalue analysis mode shape.

338   For CFG1 it was recognized that the first mode shape, illustrated in Fig. 11, matched the one

339   experimentally observed. Imperfections were then generated on the base of this mode shape,

340   with three scaling factors (s) set at 1 mm, 2.5 mm and 5 mm. The deformed shape at the last

341   load step from the non-linear analysis is represented in Fig. 13 by a contour plot for the y-

342   displacements. It is observed that the deformed shape is similar to the first mode shape in Fig.

343   11, calculated by the Eigenvalue analysis. The predicted ultimate load is found to be 178 to

344   213 kN, depending on the scaling factor s; the higher the value of s the lower the resistance of

345   the built-up column is. The failure load was taken as the load in the numerical solution when

346   there was a loss of static equilibrium and an absence of convergence at the next load step.

347   From column-type CFG2 the mode shapes of interest to define the geometric imperfections

348   were the first and third. These modes from the Eigenvalue analysis are illustrated in Parts (a)

349   and (c) of Fig. 12. The second mode shape, shown in Fig. 12(b), cannot be physically

350   activated because of the mechanical interaction (for the composite action) between the flange

351   and the web prevents an inner (towards the web) deflection of the 9.5 mm thick flange

352   channel. In order to eliminate any activation of the second mode shape contact pairs between

353   the thicker flange of 9.5 mm thickness and the 6.5 mm web Cs are introduced along the full

354   column height. This FE modeling feature is shown in Figure 14. Since a gap is present in the

355   FE mesh between web and flanges (because shell elements are located at the mid-surfaces of

356   their thin-walls) the "close initial gap" option is activated for contact modeling (Ansys 2011).

357   In order to activate the first buckling mode in the non-linear analysis with CFG2 it was

358   necessary to apply the geometric imperfection defining this mode shape with s equal to 5

359   mm. Three scaling factors of $s = 1$ mm, 2.5 mm and 5 mm were employed for the equivalent

360   imperfection associated with the third mode shape, as shown in Fig. 12(c).

361   The deformed shape at the last load step is represented in Fig. 15, together with a contour plot

362   of the displacements in the x-direction (left-sided) and y-direction (right-sided). The

363   deformed shape is characterized by lateral deformation of the thinner (6.5 mm) flange in the

364   x-direction and of the web in the y-direction. The ultimate load is found to be 45 to 56 kN,

365   depending on the scaling factor s chosen for the third mode shape; again, the larger s is the

366   lower is the resistance.

367

Comparison between numerical and test results

Table 3 is used to make a comparison between the experimental and numerical determined resistances of columns CFG1 and CFG2. Column (1) gives the label for the six specimens and Column (2) reports their ultimate test load, and when occurring their buckling load, which is given between parentheses. Columns (3) and (4) give the flexural buckling resistance as determined by the Euler and Engesser closed form equations, respectively. By including shear deformation, P_{Esh} (from Equation (1)) is about 5% lower; a similar percentage reduction with concentrically loaded pultruded columns of H-shapes has been established by Mottram *et al.* (2003). Columns (5) and (6) present the bifurcation and non-linear FEA results employing the modelling methodology introduced above. Section properties are taken from Table 1 and the elastic constants are from Table 2 (they were not determined using coupons cut from the C sections in the built-up specimens).

A form of buckling failure was not realised with configuration CFG1 in tests 1 and 2. The experimental ultimate loads of 148 kN and 249 kN were established by local compressive crushing of the web at one end. The considerable difference of 68% (or 101 kN) is solely due to the technical challenge of ensuring there is a uniform distribution of the load over the web's total area of 3000 mm^2. A possible reason for why the failure load in test 2 exceeded the upper bound Eigenvalue buckling load of 230 kN is that the shape of the out-of-straightness imperfection for Minor-axis flexural buckling at the beginning of testing was for a higher mode. Supporting this proposal is the similar experimental response reported from test number 11 (H-profile of 152x152x9.53 mm at length 3300 mm) in the series of concentrically loaded column tests by Mottram *et al.* (2003).

The ultimate and buckling load of 193 kN from CFG1 test 3 is seen to be 85% of the critical load of 230 kN by the Eigenvalue FEA. A higher critical elastic buckling load is to be

392 expected from an Eigenvalue analysis because the influence of the imperfections present in

393 testing will ensure the measured resistance is lower, if not significantly so. It is observed that

394 the buckling shape established in the FEA and presented in Fig. 11 is found to correspond to

395 that visually observed in CFG1 test 3.

396 It is found that the FEA bifurcation load is 70% of the Engesser flexural buckling resistance

397 of 331 kN. This latter is computed under the hypothesis of full composite action, whereas the

398 degree of mechanical interaction between the four channels is taken into account in the FE

399 analysis, leading to a lower buckling load that is found to be closer to the experimental

400 buckling load. This finding suggests that FEA is required to establish the buckling resistance

401 of built-up compression struts when the degree of composite action between individual

402 sections has a significant role in controlling structural performance.

403 In Fig. 16 the test data from CFG1 tests 1 to 3 for the y-displacement at mid-height is

404 compared with the equivalent non-linear prediction for a compressive force to ultimate

405 failure. Unfilled symbols are for experimental results (square for test 1, triangle for test 2 and

406 rhombus for test 3), while filled symbols are for FE results (square for $s = 1$ mm, triangle for

407 $s = 2.5$ mm and rhombus for $s = 5$ mm). For the FEA curves the three scaling factors are for

408 the imposed geometric imperfections in mesh specification. It can be seen that the range of s

409 values is able to simulate reasonably well the non-linear stiffness behaviour; it is noted that

410 each specimen needs a different s and crushing failure is not captured.

411 Let's now consider the same comparison for column configuration CFG2. From testing it was

412 found that a form of buckling failure was not achieved in test 3. The bifurcation load of 39

413 kN in Column (5) of Table 3 is seen to be within 1 kN of the experimental ultimate load

414 achieved in the other two tests. For CFG2 tests 1 and 2 the load-axial displacement curves in

415 Figs. 6 and 7 show that there was a stable post-buckling branch. The FEA predicted buckling

416 shape shown in Fig. 15 is similar to that visually observed in these two tests.

17

417   In Fig. 17 the test results for column configuration CFG2 are compared with the non-linear

418   FEA outputs. The format of the figure is the same as in Fig. 16 for the CFG1 columns, except

419   that the three scaling factors (i.e. s set at 1 mm, 2.5 mm or 5 mm) are for the third buckling

420   mode shape (see Fig. 12(c)). A constant scaling factor of 5 mm was applied to the geometric

421   imperfection of a half sine wave along the column length for the first mode shape. It can be

422   seen that with scaling factors of 1 and 2.5 mm with the third mode the computational curves

423   tend to fit the measured response of test 2. Modelling requires s to be set to 5 mm for the

424   FEA curve to correspond to what was found in test 1.

425

426   **CONCLUDING REMARKS**

427   A fact finding study has been made on the structural response of a built-up column (envelop

428   is 152 x 171 mm) of length 2.734 m subjected to (concentric) compressive loading. To

429   understand the behavior the study combined physical testing and (linear elastic material)

430   numerical approaches. Mechanical performances from three columns, for the configuration

431   that is similar to the strut members in the FRP structure inside the church of Santa Maria

432   Paganica in L'Aquila, were found to be dependent on the end boundary conditions. Two of

433   these specimens ultimately failed at one end, by material crushing in the two channel sections

434   forming the web (there is no loading applied into the two flange channel sections). This result

435   was not expected *a proiri*, and its presence highlights the sensitive of FRP materials to

436   localized failure where concentrated forces are transferred into (and out of) members.

437   In a third test the mode of failure was by global flexural buckling when the compression force

438   was 193 kN. Numerical predictions of 230 kN by Eigenvalue FEA and 331 kN from the

439   Engesser closed form equation were much higher; even when the moduli of elasticity where

440   design manual value that are known to be lower than actual. This finding suggests that there

441   is not full composite action between the four channel sections, and opens up the possibility

442   that with additional bolting, say at the sixth length locations, the column buckling strength

443   can be further enhanced. Moreover, by combining experimental and numerical results it is

444   observed that imperfections, geometric and from other sources, have an important role in

445   establishing the structural performance of the built-up columns.

446   From non-linear FEA the ultimate compressive load was in the range 178 to 213 kN

447   depending on the magnitude of the scaling factor in the FE modelling used to define the

448   amplitude of geometric imperfections. This was found to bound the measured buckling

449   resistance from test 3. In the FE modelling it was found that by increasing the scaling factor

450   from 1 to 5 mm there was a decrease in both critical elastic buckling load and the members'

451   initial axial stiffness. A numerical prediction was observed to be close to what was measured

452   when the scaling factor was either 2.5 or 5 mm. The initial stiffness was found to be

453   underestimated by FEA, unless the lowest geometric imperfection scaling factor of 1 mm was

454   applied. It was established that the computed buckled shape corresponds to that visually

455   observed in test 3.

456   By removing the two rows of bolted connections at the third lengths the much lower column

457   resistance of about 40 kN was determined in two of the three tests with this column

458   configuration. Material crushing at one end was one reason why the three nominally identical

459   columns failed differently. A critical elastic buckling load of 39 kN was predicted by

460   Eigenvalue FEA. It can be concluded that the bolting at third lengths was sufficient, and

461   necessary, for the built-up member to have column strength that was five times higher than if

462   the built-up strut is without the composite action. The largest scaling factor of 5 mm for the

463   first mode shape was found to be the 'lowest' that would activated this mode in the non-linear

464   FEA.

465   A reasonable, but not good, agreement between the equivalent numerical and the

466   experimental results was observed prior to the first non-linear branch and before buckling

467   deformation occurred. The post-buckling stage that followed in testing had a stable branch

468   that cannot be reliably simulated by FEA. Up to a mid-height lateral displacement of 13 mm

469   (or 1/200 of column height) there was little difference between FEA and testing for flexure

470   occurring about the minor-axis. Continuing to increasing load it was found that the deviation

471   in load-displacement response between the test columns in a group of three may become very

472   significant. The numerical-experimental comparison reported in this paper has shown that the

473   response of built-up FRP members could be challenging to reliably predict by FEA.

474

475   **REFERENCES**

476   Anonymous (2011). *ANSYS® Multiphysics, Release 14.0, Help System*, ANSYS Inc.

477   Bank, L. C. (2006). *Composites for Construction - Structural Design with FRP Materials*,

478   John Wiley & Sons, N.J.

479   Barbero, E. J., Dede, E. K., Jones, S. (2000). "Experimental Verification of Buckling-mode

480   Interaction in Intermediate-length Composite Columns", *International Journal of Solids and*

481   *Structures*, 37(29), 3919-3934.

482   Boscato, G. and Russo, S. (2009). "Free Vibrations of Pultruded FRP Elements: Mechanical

483   Characterization, Analysis, and Applications", *Journal of Composite for Construction*,

484   ASCE, 13(6), 565-574.

485   Boscato, G., Mottram, J., Russo, S. (2011). "Dynamic Response of a Sheet Pile of Fiber-

486   Reinforced Polymer for Waterfront Barriers", *Journal of Composite for Construction*, ASCE,

487   15(6), 974–984.

488   Di Tommaso, A. and Russo, S. (2003). "Shape Influence in Buckling of GFRP Pultruded

489   Columns", *Mechanics of Composite Materials*, 39(4), 329-340.

490   Engesser, F. (1889). "Ueber die Knickfestigkeit gerader Stabe", *Zeitschrift für Architekter*

491   *und Ingenieurwsen*, 35(4), 455-462 (in German).

Fiberline design manual for structural profiles in composite materials. (2013). *Fiberline Composites A/S*, Kolding, Denmark.

Hashem, Z. A. and Yuan, R. L. (2001), "Short vs. Long Column Behavior of Pultruded Glass-fiber Reinforced Polymer Composites", *Construction and Building Materials*, 15(8), 369-378.

Lane, A. and Mottram, J.T. (2002). "The Influence of Modal Coupling upon the Buckling of Concentrically Pultruded Fibre-reinforced Plastic Columns", *Proceedings of the Institution of Mechanical Engineers Part L: J. Materials - Design and Applications*, 216 133-144.

Mottram, J. T. (2004). "Determination of Critical Load for Flange Buckling in Concentrically Loaded Pultruded Columns", *Composites*: *Part B Engineering*, 35 35-47.

Mottram, J. T. (2011). "Does Performance Based Design with Fibre Reinforced Polymer Components and Structures Provide any new Benefits and Challenges?", *The Structural Engineer*, 89(6), 23-27.

Mottram, J. T., Brown, N. D. and Anderson, D. (2003). "Physical Testing for Concentrically Loaded Columns of Pultruded Glass Fibre Reinforced Plastic Profile", *Structures and Buildings*, 156(2), 205-219.

Pecce, M. and Cosenza, E. (2000). "Local Buckling Curves for the Design of FRP Profiles", *Thin-Walled Structures*, 37(3), 207-222.

Russo, S. (2012). "Experimental and Finite Element Analysis of a Very Large Pultruded FRP Structure Subjected to Free Vibration", *Composite Structures*, 94(3), 1097-1105.

Russo, S. (2007). Strutture in Composito: Sperimentazione, Teoria e Applicazioni, Edited by Ulrico Hoepli, Milano, Italy (in Italian).

Russo, S., Boscato, G. and Mottram, J. T. (2012). "Design and Free Vibrations of a Large Temporary Roof FRP structure for the Santa Maria Paganica Church in L'Aquila, Italy".

516 Presented at *6th International Conference on FRP Composites in Civil Engineering (CICE*

517 *2012)*, Section 8: All-FRP and Smart FRP Structures, Paper 209, 13th-15th June 2012.

518 Turvey, G. J. and Zhang, Y. (2006). "A Computational and Experimental Analysis of the

519 Buckling, Postbuckling and Initial Failure of Pultruded GRP Columns", *Computers and*

520 *Structures*, 84(22-23), 1527-1537.

521

522

523   Table 1. Physical and geometric properties of four channel profiles.

Property (1)	Notation (2)	Value	
		Nominal (3)	Exp. (4)
Cross-sectional area of column	A	83.2 cm^2	65.8 cm^2
Minor-axis second moment of area	I_x	1370 cm^4	1250 cm^4
Major-axis second moment of area	I_y	3550 cm^4	2840 cm^4
Minor-axis shear area	$A_{s,x}$	37.1 cm^2	26.6 cm^2
Major-axis shear area	$A_{s,y}$	47.7 cm^2	38.6 cm^2
Bulk weight density of FRP		1850 kg/m^3	
Volume fraction of E-glass fibre		48%	

524
525
526

527   Table 2. Elastic constants for the C-shape section (Fiberline 2013).

Definition (1)	Notation (2)	Value (3)
Longitudinal modulus of elasticity	E_z	23 GPa
Transverse modulus of elasticity	$E_x = E_y$	8.5 GPa
Transverse shear modulus of elasticity	G_{xy}	3.4 GPa
In-plane shear modulus of elasticity	$G_{zx} = G_{zy}$	3 GPa
Major Poisson's ratio	$v_{zx} = v_{zy}$	0.23
Minor Poisson's ratio	v_{xy}	0.09

528
529
530
531
532

533   Table 3. Ultimate test loads and numerical elastic loads.

Column specimen (1)	Ultimate test load (buckling load) [kN] (2)	Flexural buckling load from Euler $P_E = \dfrac{\pi^2 EI}{(kl)^2}$ [kN] (3)	P_{Esh} Equ. (1) [kN] (4)	Eigenvalue buckling load [kN] (5)	Non-linear FEA ultimate load [kN] (6)
CFG1 test 1	148				
CFG1 test 2	249			230	178-213
CFG1 test 3	193 (193)	349	331		
CFG2 test 1	123 (40)				
CFG2 test 2	118 (40)			39	46-56
CFG2 test 3	122				

534
535

536

Figure 1. Temporary FRP structure for Santa Maria Paganica church: (a) overall construction;
(b) details of bolted gusset plate for frame joints.

539
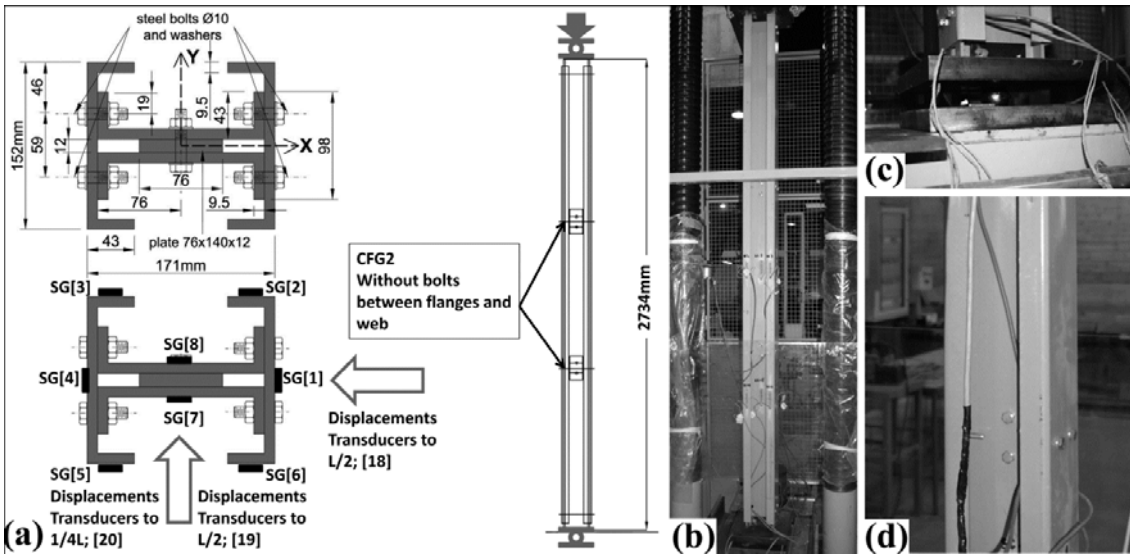
Figure 2. Details of PFRP built-up columns: (a) member cross-section and scheme for
column testing; (b) actual test set-up; (c) detail of hinge end constraints; (d) M10 steel bolting
for composite action between the four C-sections.

545

24
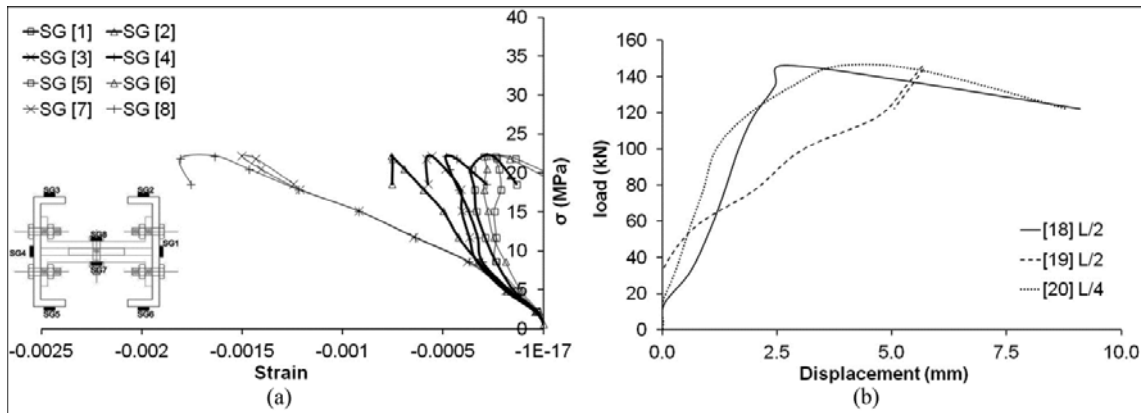
Figure 3. CFG1 test 1: (a) eight direct stress-direct strain curves; (b) three load-lateral displacement curves.
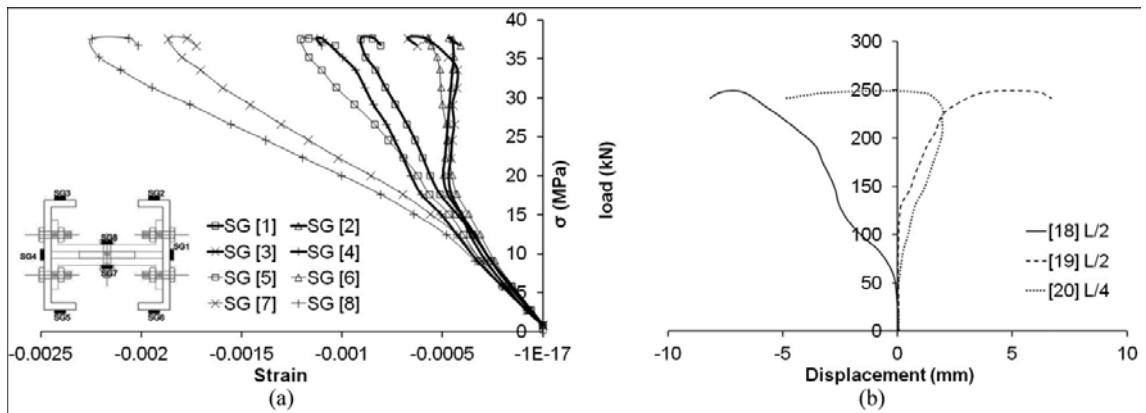
Figure 4. CFG1 test 2: a) eight direct stress-direct strain curves; (b) three load-lateral displacement curves.
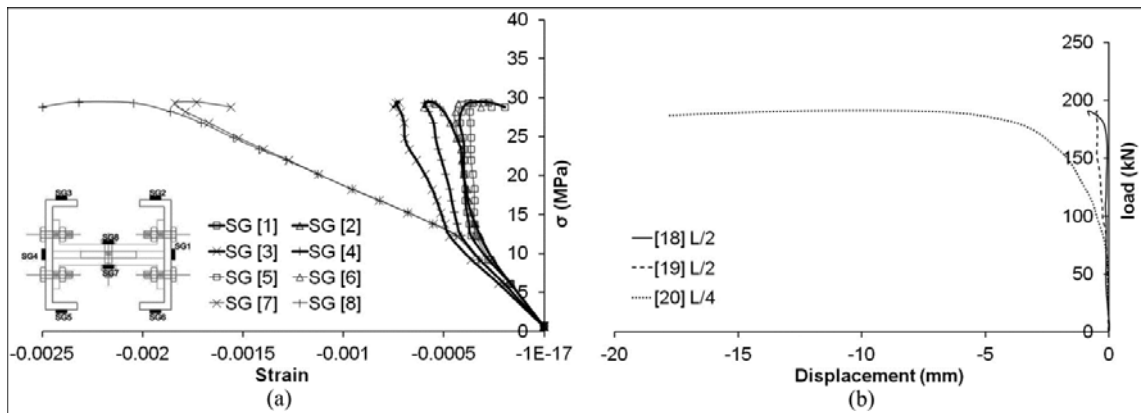
Figure 5. CFG1 test 3: a) eight direct stress-direct strain curves; (b) three load-lateral displacement curves.

558
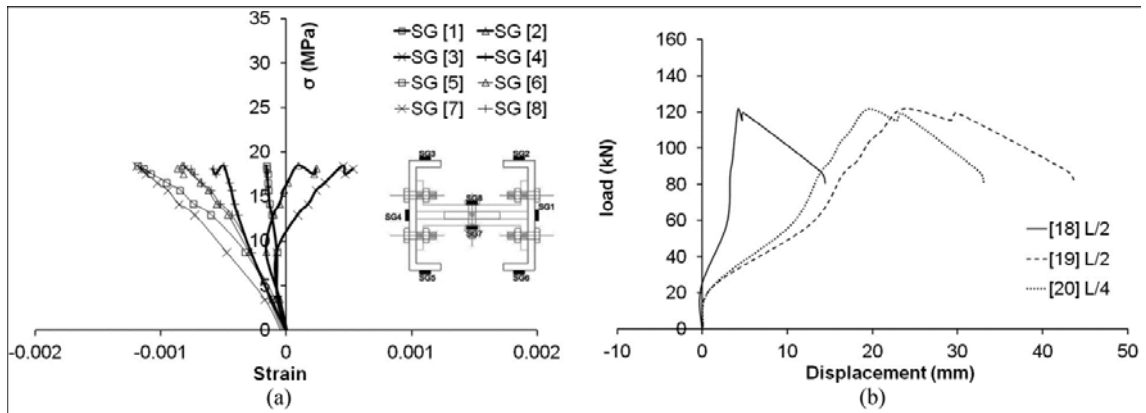
559 Figure 6. CFG2 test 1: a) eight direct stress-direct strain curves; (b) three load-lateral
560 displacement curves.

561

562
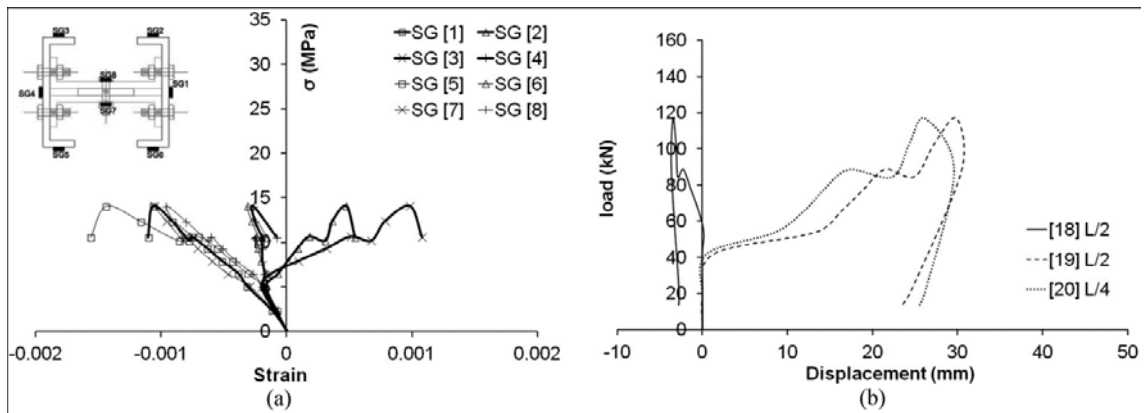
563 Figure 7. CFG2 test 2: a) eight direct stress-direct strain curves; (b) three load-lateral
564 displacement curves.
565

566
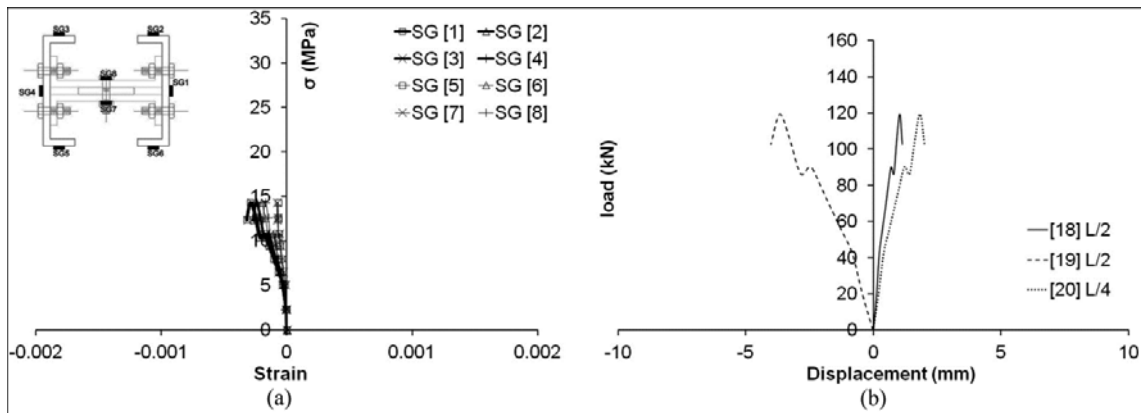
567 Figure 8. CFG2 test 3: a) eight direct stress-direct strain curves; (b) three load-lateral
568 displacement curves.
569

26

(a)   (b)
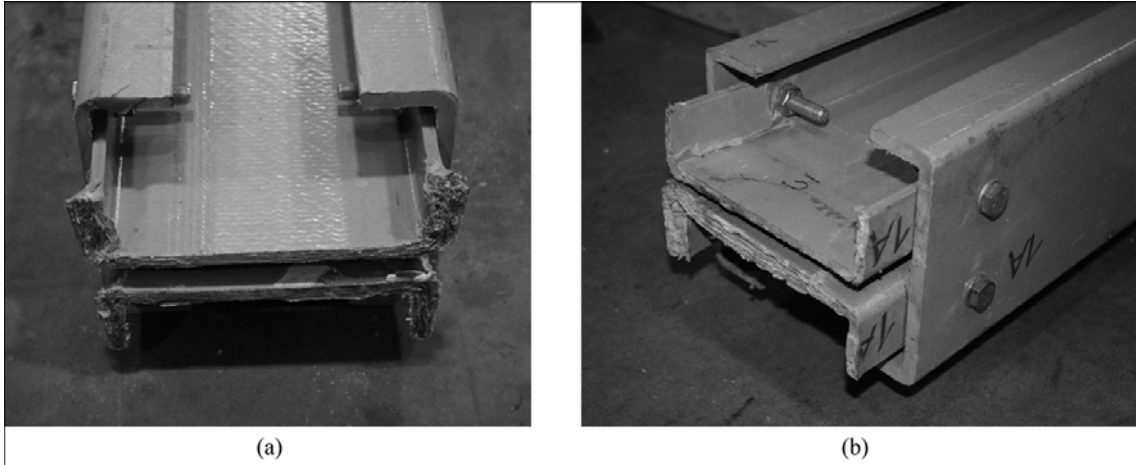
Figure 9. Local end-crushing in column-type CFG1: (a) test 1; (b) test 2.

9.5 mm thick flange

6.5 mm thick flange
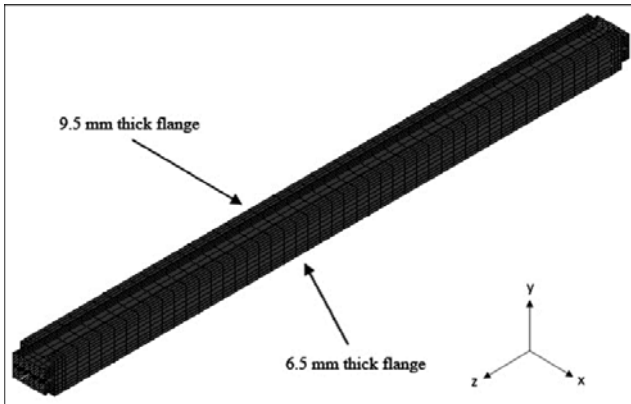
Figure 10. Isometric view of finite elements mesh for built-up column defined in Figure 2.
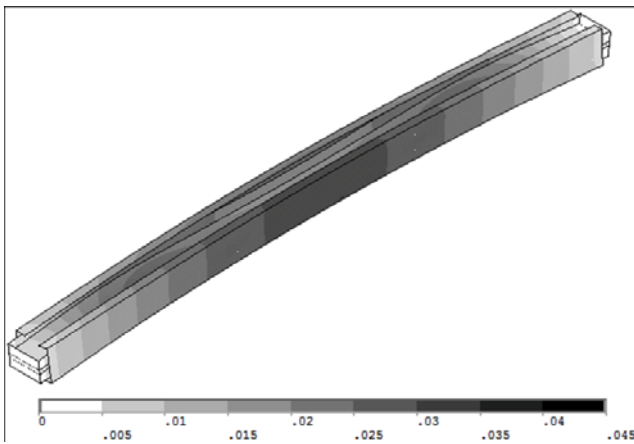
Figure 11. Eigenvalue first mode shape with contour plot for lateral y-displacement for column configuration CFG1.

584
585
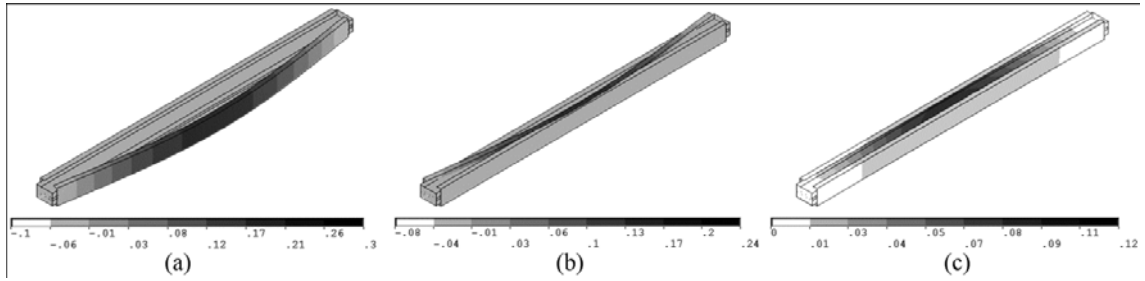
586 Figure 12. Eigenvalue first mode shape (a), second mode shape (b) and third mode shape (c)
587 with contour plot for lateral *x*-displacement (a-b) and *y*-displacement (c) for column
588 configuration CFG2.

589
590
591

592
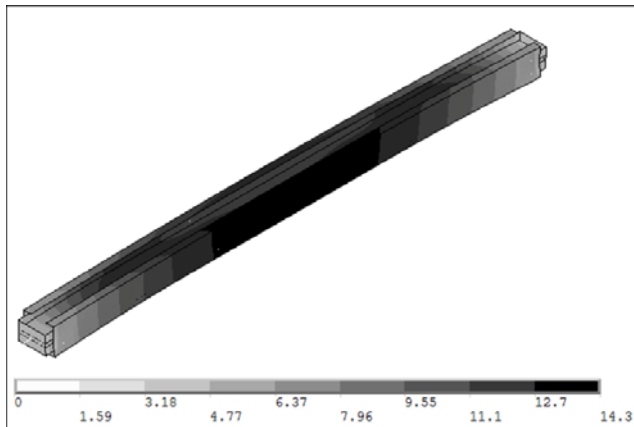
593 Figure 13. Non-linear FEA deformed shape via lateral *y*-displacement (mm) for configuration
594 CFG1.

595
596

597
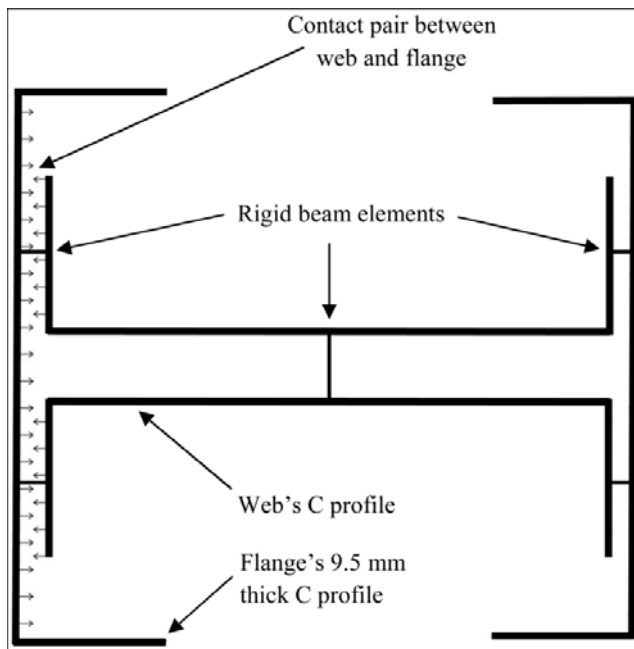
598 Figure 14. Locations for contact pairs between web and flange and for rigid-beam elements
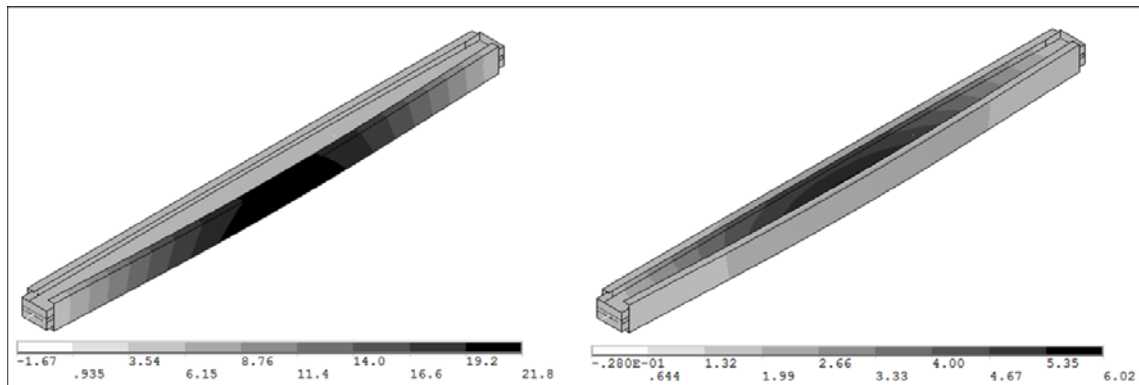599 for the bolted connections when modelling column-type CFG2.
600
601

602

603 Figure 15. Non-linear FEA deformed shape using lateral x-displacment (left) and y-
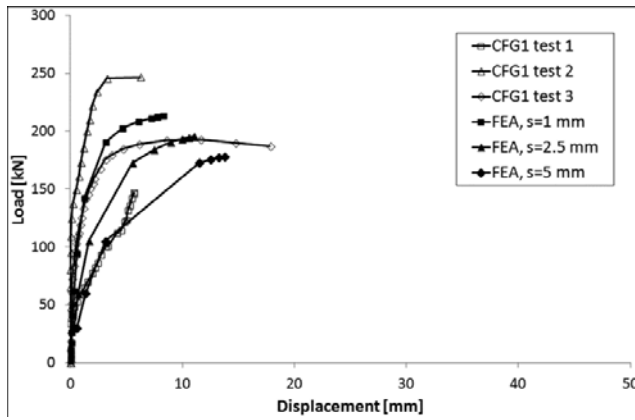604 displacement (mm) (right) for configuration CFG2.
605
606
607

608
609

Figure 16. Experimental and non-linear FEA *y*-displacements with compression force at mid-height for CFG1. FEA results with three factors *s* for the geometric imperfection for the first mode shape.
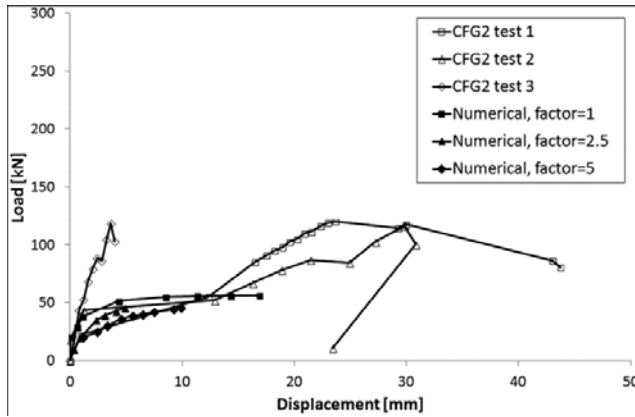
613
614

615
616

Figure 17. Experimental and non-linear FEA lateral *y*-displacements with compressive load for CFG2 at mid-height. FEA results with three factors *s* for the geometric imperfection for the third mode shape.